AGU100 ADVANCING EARTH AND SPACE SCIENCE

Water Resources Research

RESEARCH ARTICLE
10.1029/2017WR021875

Key Points:
- Fast lateral drainage in early wet season and high vertical groundwater recharge in late wet season explain land use effects on runoff
- Core-scale infiltrability and plot-scale infiltration capacity allow estimating a number of vertical macropores that fully penetrate root zone
- A physically based model allows causal attribution in land use/land cover effects to preferential flow

Correspondence to:
J. Zhu and Y. Cheng,
jzhu5@uwyo.edu;
yanyan.cheng@pnnl.gov

Citation:
Cheng, Y., Ogden, F. L., Zhu, J., & Bretfeld, M. (2018). Land use-dependent preferential flow paths affect hydrological response of steep tropical lowland catchments with saprolitic soils. *Water Resources Research*, *54*, 5551–5566. https://doi.org/10.1029/2017WR021875

Received 15 SEP 2017
Accepted 10 JUL 2018
Accepted article online 18 JUL 2018
Published online 17 AUG 2018

Land Use-Dependent Preferential Flow Paths Affect Hydrological Response of Steep Tropical Lowland Catchments With Saprolitic Soils

Yanyan Cheng[1,2], Fred L. Ogden[1,3,4], Jianting Zhu[1], and Mario Bretfeld[4]

[1]Department of Civil and Architectural Engineering, University of Wyoming, Laramie, WY, USA, [2]Now at Atmospheric Sciences and Global Change Division, Pacific Northwest National Laboratory, Richland, WA, USA, [3]U.S. National Water Center, NOAA/NWS/Office of Water Prediction, Tuscaloosa, AL, USA, [4]Smithsonian Tropical Research Institute, Ancón, Panama

Abstract Forested catchments in Central Panama can produce more base flow during the dry season compared to pasture catchments—the so-called "forest sponge effect." During rainfall events, peak storm runoff rates and storm runoff coefficients can be lower for forested catchments than pasture catchments, even when they have similar topographic characteristics, underlying geology, and soil texture. The internal mechanism of these differences in hydrological response due to land use is yet to be fully understood. A distributed model explicitly simulating preferential flow paths (PFPs), which is referred to as "PFPMod," is used to explain the hydrological response caused by land use using data from three catchments with distinct land covers in Central Panama. Input parameters of forest and pasture land covers were identified using field observations and literature values. Multiple satisfactory objective criteria demonstrate that the two end-member land cover parameter sets are adequate to explain the observed difference in dry-season base flow and storm runoff coefficients. Field measurements of matrix infiltrability using soil cores and plot-scale infiltration capacity enabled estimating the number of vertical macropores that fully penetrate the root zone. Model simulation results demonstrate that fast drainage through lateral PFPs in the early wet season and high flow in vertical PFPs to recharge deep groundwater in the late wet season contribute to the observed differences in peak storm runoff and the "forest sponge effect" during the dry season. This study provided insights to the mechanism by which reforestation may help to restore ecosystem services and water security in tropical settings.

1. Introduction

Tropical water supplies are often affected by streamflow seasonality, droughts, land degradation (Bai et al., 2008), old or nonexistent infrastructures, and increasing water demand due to rapid population growth (Bonell & Bruijnzeel, 2005). Water shortages are most acute in the 80% of the tropics with an extended dry season (Peel et al., 2007). Due to climate change, longer dry periods and more frequent severe droughts are expected (Bernstein et al., 2008). These factors taken together indicate the vulnerability of water supplies in the seasonal tropics.

Land management aiming at improving hydrological ecosystem services represents one potential way to mitigate drought effects. However, hydrological processes and functioning of tropical forests are complicated (Bonell & Bruijnzeel, 2005; Chappell, 2010) and relatively little is known about the dominant water flow paths and characteristics of quick flow and base flow in the humid tropics (Chappell et al., 2007). In particular, the influence of land use/cover changes (LUCCs) on the hydrological behavior of tropical catchments is complicated by multiple interrelated processes as LUCC can directly or indirectly influence such as cloud cover, albedo, evapotranspiration, soil moisture, vegetation water use, and streamflow (Ray et al., 2006; Wu et al., 2007). Studies of LUCC in tropical ecosystems are also relatively scant in contrast to more comprehensively studied temperate catchments (Birkel et al., 2012). For example, the "infiltration-evapotranspiration trade-off hypothesis" (Bruijnzeel, 1989, 2004) that examines the extent to which reforestation can enhance the dry-season base flow under seasonal tropical conditions is yet to be adequately studied (Krishnaswamy et al., 2012, 2013). This creates a management need for predictive understanding of the effects of LUCC on hydrological responses in tropical settings.

While direct field observations can assess the hydrological impact of LUCC (Bruijnzeel, 1989; Ghimire et al., 2014; Ogden et al., 2013), modeling studies can provide additional insights and flexibility in addressing the

underlying mechanism of watershed hydrological response due to LUCC (Bruijnzeel, 2004; Li et al., 2007). Relatively simple models (Beck et al., 2013; Chappell et al., 2007; Lacombe et al., 2016) have been applied more frequently than fully physically based models to understand runoff generation in tropical forests (Cheng et al., 2017; Schellekens, 2000; Vertessy & Elsenbeer, 1999) and changes therein after LUCC (Birkel et al., 2012; Li et al., 2007). The work of Lacombe et al. (2016) in Laos and Vietnam showed that a simple two-parameter model can be adequate when predicting changes in water yield during vegetation succession or plantation growth by taking annual variability in rainfall into account. However, physically based, distributed models can allow a greater understanding of specific internal mechanisms of hydrological processes associated with LUCC (Bonell & Bruijnzeel, 2005) The physically based model proposed in Sarkar et al. (2012) gave a quantitative indication of hydrologically active lateral macroporosity of the hillslope and the dependency of effective lateral macroporosity, soil matrix, and macropore flow rates on recharge rate in Northeast India. The hillslope model developed in Sarkar and Dutta (2014) examined the effect and sensitivity of landscape physiography, rainfall intensity, infiltration rates, and soil macropore structures on overland flow and subsurface flow responses on a nested hillslope in Northeast India. The physically based model advanced in Cheng et al. (2017) included four different optional model structures without and with explicit simulation of preferential flow paths (PFPs). The model was used to test hypotheses and identify plausible hydrological processes in a steep, saprolitic, and tropical lowland catchment in the Panama Canal Watershed. This model allowed exploration of the effects of both lateral and vertical PFPs on the hydrological response. Results by Cheng et al. (2017) showed the role of lateral PFPs in contributing to quick flow and the role of vertical PFPs in controlling groundwater recharge. These findings were supported by geochemical tracer studies (Litt et al., 2015) and shallow subsurface flow path activation identified using Ge/Si as a tracer (Gardner et al., 2017).

Accurate measurement of infiltration parameters in macropore-dominated catchments is critical for physically based hydrological modeling. Mallants et al. (1997) evaluated the spatial variability of saturated hydraulic conductivity (K_{sat}) in soils with macropores using different column sizes and discovered the geometric mean of K_{sat} decreased with increasing column size. By comparing model- and core-derived block permeability estimations, Chappell et al. (1998) concluded that there was a nonlinearity between the watershed hydrological response and the block or whole-hillslope permeabilities obtained from core-scale observations. Hassler et al. (2011) reported a median soil matrix infiltrability of approximately 2 cm/hr at a depth of 6–12 cm in pasture and secondary forest land covers ranging in age from 5 to 100 years using permeability measurements from 9-cm diameter soil cores in the same Agua Salud project catchments in Central Panama used in this study. However, plot-scale field tests conducted at the same study sites using simulated rainfall on a 12-m^2 plot, which accounts for the effect of PFPs (Ogden et al., 2014), measured much higher infiltration rates than the infiltrability reported by Hassler et al. (2011) in all land covers. Sarkar et al. (2008) measured local-scale infiltration using double-ring infiltrometers and plot-scale infiltration using a sheet flow generation system in a macropore-dominated hillslope. Their results clearly indicated that the point-scale measurements led to erroneous results that were not reliable for use in hydrological modeling, while results from plot-scale experiments more accurately described infiltration processes. Davis et al. (1999) highlighted the effect of using differently derived hydraulic conductivities (small cores, large cores, and well permeametry) in hydrological modeling and demonstrated that the K_{sat} estimated from large cores captured catchment hydrological response. Therefore, physically based hydrological model studies in macropore-abundant regions should take field measurements at both small local-scale and large plot scale into account.

In addition, biological activity on/in soils is affected by LUCC, which subsequently affects the formation of PFPs, and should be considered in physically based hydrological modeling (Colloff et al., 2010; Shougrakpam et al., 2010). Many studies reported the impact of land use conversion and succession on the creation/destruction of PFPs through root growth, root decay, earthworms (Colloff et al., 2010; Meng et al., 2016; Tobón et al., 2010; Zou & Gonzalez, 1997), soil shrink/swell, and many other effects of land use (Beven & Germann, 2013). Strategies are required to incorporate catchment characteristics such as soil physical properties (Davis et al., 1999; Noguchi et al., 1997, 1999; Sarkar & Dutta, 2014; Sarkar et al., 2015; Zimmermann et al., 2006; Zwartendijk et al., 2017) into hydrological models, especially the parameters related to PFPs (Guo & Lin, 2017; Shougrakpam et al. 2010; Meng et al., 2016) as a function of land use/land cover.

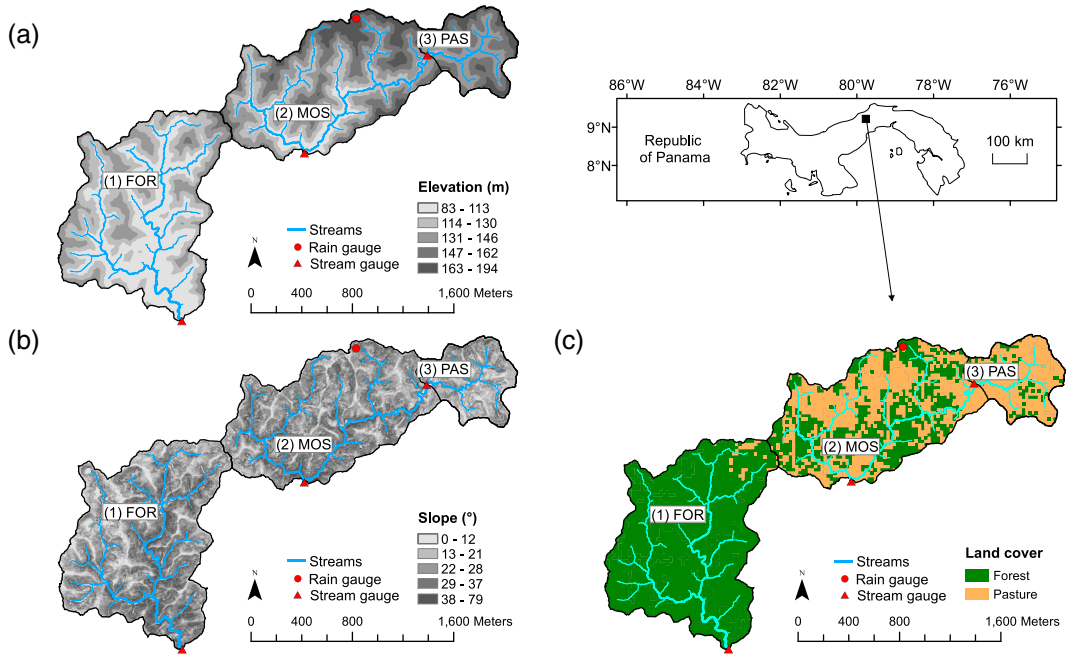

Figure 1. (a) Elevation, (b) slope, and (c) land cover of the three study catchments: (1) forest catchment (FOR), (2) mosaic catchment (MOS), and (3) pasture catchment (PAS).

The overall objective of this study was to better understand the underlying physical mechanisms behind the forest sponge effect-increased dry-season base flow in forested catchments, and the reasons for differences in peak runoff rates and runoff ratios in catchments with different land uses/land covers that were observed in Ogden et al. (2013) in Central Panama. We proposed two hypotheses: First, the dominant impact of land use/land cover on hydrological response in seasonal humid tropical catchments with saprolitic soils is through its effects on the formation of PFPs formed by plants, animals, and soil shrink/swell. Second, soil infiltrability measurements using small cores combined with infiltration measurements on plot scale allow estimation of the number of vertical macropores that fully penetrate the root zone.

We applied a physically based distributed model that we call "PFPMod" (Cheng et al., 2017) to predict and simulate runoff generation and flow paths in three steep, saprolitic, and tropical lowland catchments with distinct land covers within the Panama Canal Watershed. Different from other studies on the hydrological effect of LUCC, this study explicitly took into account the effect of LUCC on the formation of PFPs informed by the results of field measurements at core and plot scales and the literature. We evaluated the model performance in terms of event-scale runoff, base flows, and the annual water balance. Examination of multiple simulated water budget components, temporal dynamics of transient perched groundwater table depth in the upper soil layer, and flow through the fully penetrated vertical PFPs in both dry and wet seasons allowed us to gain better understanding of the effects of land use-dependent PFPs on hydrological responses.

2. Methods

2.1. Study Area

Most of the observed data used in this study were from the Smithsonian Tropical Research Institute (STRI) Agua Salud project study catchments in Central Panama. The Agua Salud project instrumented catchments with a variety of land uses: old (>100-years) primary forest, secondary forest of various ages, native tree plantations, and silvopastoral and traditional swidden pasture catchments. The baseline hydrological investigation by Ogden et al. (2013) examined three Agua Salud control catchments with similar distributions of slope and topographic index (Figures 1a and 1b), similar underlying bedrock geology but distinct land uses/land covers (Figure 1c). These three catchments also have similar soil textures as the silty texture of the soils is determined by the saprolite from which the soil is derived. These catchments include the

Table 1
Catchment Characteristics

Catchment name	FOR	MOS	PAS
Contributing area (ha)	143	183	42
Stream gauge latitude (°)	9.20893°N	9.21860°N	9.22611°N
Stream gauge longitude (°)	79.77950°W	79.77047°W	79.76166°W
Elevation range (m)	53–166	88–195	120–188
Slope range (°)	6–37	6–32	6–29
Mean topographic index	4.41	4.48	4.59
Soil taxonomy	Oxisols	Oxisols	Oxisols
Annual rainfall (mm)	3,600	3,600	3,600
Annual streamflow (mm)	1,443	2,018	2,355
Annual base flow as percent of annual streamflow (%)	78	70	57
Base flow as percent of streamflow during the dry season (%)	98	98	96
Base flow as percent of streamflow during the wet season (%)	72	65	55
Annual quick flow as percent of annual streamflow (%)	22	30	43
Quick flow as percent of streamflow during the dry season (%)	2	2	4
Quick flow as percent of streamflow during the wet season (%)	28	35	45

Note. The FOR represents for forest, MOS represents for mosaic, and the PAS represents for pasture.

following: (1) 143 ha covered by old (>100-years) regrowth forest (FOR catchment), (2) 183 ha covered by a mosaic of secondary succession and pasture (MOS catchment), and (3) 42 ha active pasture (PAS catchment), which is a subwatershed of the mosaic catchment (Figure 1), managed with rotational grazing and manual shrub removal once per year. Note that the areas of these catchments differed slightly from those reported in Ogden et al. (2013), as a result of improved Digital Elevation Model (DEM) data availability (Robert F. Stallard, personal communication, 2017). The characteristics of the three study catchments are summarized in Table 1.

The three catchments experienced highly correlated rainfalls owing to their close proximity and small size, and therefore, rainfall data from the same station was used (Figure 1). Rainfall data for a period of one entire water year (11 May 2011 to 19 May 2012) covering both wet and dry seasons with a 15-min temporal resolution were used to drive the model simulations for the three study catchments. The cumulative rainfall was 3,600 mm during this study period (Table 1). The average rainfall intensities for the early wet season from May to early October, the late wet season from late October to December, and the dry season from January to April were 7.6, 6.7, and 3.0 mm/hr, respectively.

Flows from these three catchments were measured using two stage weirs as described in Ogden et al. (2017). Ogden et al. (2013) reported distinct differences in the hydrological response of these three catchments in terms of annual water balance, peak runoff rate, and runoff ratio during heavy rainfall events, and dry season base flow. This latter observation supported the "forest sponge effect hypothesis" because the forested catchment produced more base flow during the dry season than both the mosaic and pasture catchments.

2.2. Hydrological Model

This study applied PFPMod (Cheng et al. 2017), which was developed to simulate the hydrological response of steep, saprolitic, and tropical catchments by explicitly simulating the influence of both lateral and vertical PFPs in a two-layered soil system. The model tested four different model structures in a near-surface layer where most abundant PFPs occur, called the "preferential flow layer." The model computed 2-D overland flow based on a DEM-based grid cell network and simulated 1-D channel flow using a DEM-based channel element network. Percolation based on the matrix hydraulic conductivity linked the preferential flow layer and deep groundwater. Deep groundwater discharge to streams was simulated using a simple linear reservoir. This study applied the best performing model structure identified by Cheng et al. (2017), which is shown schematically in Figure 2a. This model structure divided the preferential flow layer into two layers, a top layer and a sublayer. In the top layer, a simple rapid infiltration scheme assumed that all the througfall bypasses the soil matrix and immediately reaches the bottom of the top layer. The sublayer was further divided into two domains, a matrix infiltration domain and a vertical PFP domain. In the matrix infiltration domain, downward water movement was simulated using the Green-Ampt infiltration with redistribution (GAR) model with features from the Talbot-Ogden (T-O) infiltration and redistribution method (Lai et al., 2015), which is a simplified version of the finite moisture content solution of the Soil Moisture Velocity Equation (Ogden et al., 2015, 2017). Macropores in the vertical PFP domain were assumed to fully penetrate the preferential flow layer and were referred to as "effective percolating vertical PFPs." Water movement through these effective percolating vertical macropores was explicitly simulated using a laminar pipe flow equation. The best performing model structure contained about 20 parameters, but most of its input parameters can be estimated from field data or literature to minimize calibration. The best performing model structure was applied to the FOR, MOS, and PAS catchments as discussed above (Figure 1). The model initialization involved a spin-up period of one full water year for all three study catchments.

Evapotranspiration (ET) in the seasonal Panama Canal Watershed exhibits considerable intra-annual variability. ET variability is largely driven by seasonal variability of transpiration in response to seasonal

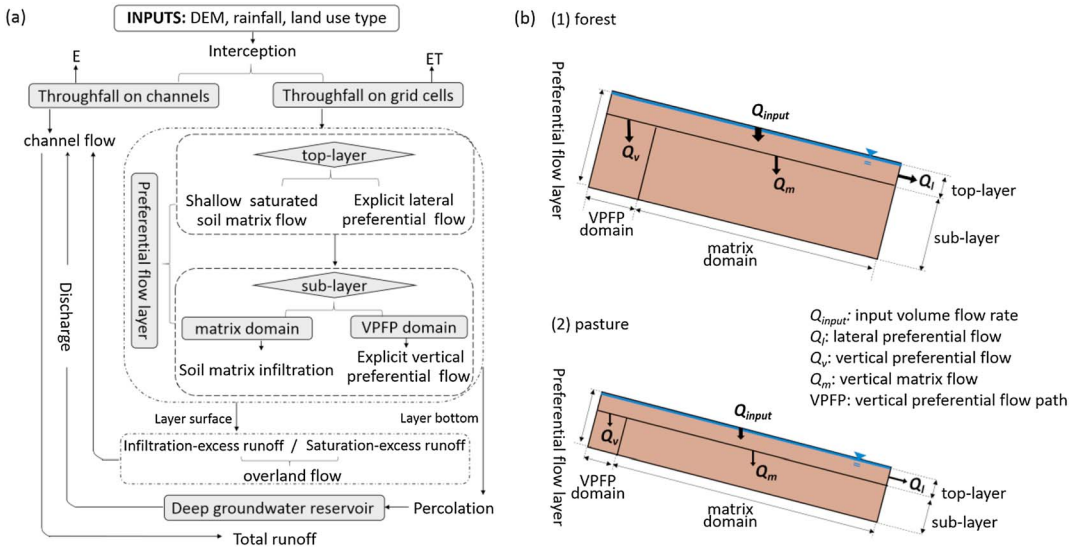

Figure 2. (a) Flow chart of the overall model computation process and (b) schematic representation of two distinct land use classes in estimating vertical PFP numbers: (1) forest land use and (2) pasture land use and water balance components used in equation (2).

differences in energy (radiation) and water (soil moisture) availability (Wolf et al., 2011). During the wet season, frequent cloud cover and low vapor pressure deficit limit transpiration despite sufficient plant-available soil moisture (Graham et al., 2003), whereas during the dry season, radiation and vapor pressure deficit increase while infrequent, reduced precipitation limits plant-available soil moisture for grasses and understory vegetation. The resulting seasonal differences in ET can be expressed as a dry-to-wet season ET ratio, with generally larger ratios in forests than in pastures (von Randow et al., 2004; Wolf et al., 2011). The typically higher dry-to-wet season ET ratio in forests is caused by elevated dry-season transpiration in forests due to increased available energy (radiation) and access to deep soil water through deeper root systems (Schwendenmann et al., 2015), whereas the low soil water content in the upper soil layer during the dry season limits transpiration of pasture vegetation with shallower root systems (Wolf et al., 2011). To estimate the dry-to-wet season ET ratio for the mature and young secondary forest, we calculated the seasonal averages of daily transpiration based on sap flow measurements from 25 and 30 trees in mature and young forest, respectively. Sap flow data were collected using the Heat-Ratio method (Burgess et al., 2001) from 1 August 2015 to 10 September 2017. Measured temperature ratios were converted to sap velocities according Burgess et al. (2001) and Marshall (1958). Sapwood areas per tree were estimated based on a diameter at breast height-to-sapwood area relationship derived from 107 trees representing 24 species in Panama (Meinzer et al., 2001). The sapwood area and sap velocities together determined the transpiration rate per tree (Bretfeld et al., 2018). The dry-to-wet season ET ratio of forest is the ratio between the average daily transpiration rates in dry and wet seasons, respectively. The dry-to-wet season ET ratio for the pasture catchment was based on ET data from a 5-m eddy flux tower located in the PAS catchment from October 2015 to May 2017. The dry-to-wet season ET ratio of pasture is the ratio between the average daily evapotranspiration rates during dry and wet season periods. In this study, the dry-to-wet season ET ratios were calculated as 1.9, 1.26, and 1.01 for mature forest (stand age $>$ 80 years), young secondary forest (stand age 8–10 years), and pasture, respectively.

While there are multiple land cover categories in the three catchments, we used only two end-members of mature forest and pasture to reduce the number of land cover-related parameters and minimize calibration. Hydrologically, we treated a major land cover type of young secondary forest as pasture given that its dry-to-wet-season ET ratio is closer to pasture, as discussed earlier. In doing so, we generated the land cover maps for the three study catchments (Figure 1c) to assign land cover type to each 25 m $\times$ 25-m model grid cell. In the FOR catchment, 99% of its total area was covered by mature forest, while pasture covered 73% of the entire catchment area in the PAS catchment. In the case of the MOS catchment, both forest and pasture

Table 2
(a) Common Parameters Used in the Overall Model Framework and (b) Land Cover Specific Parameters Related to Forest and Pasture Land Covers

(a) Common parameters	Descriptions	Values	References
n_1	Manning roughness coefficient for overland flow routing (−)	0.07	Arcement and Schneider (1989)
n_2	Manning roughness coefficient for channel routing (−)	0.03	Arcement and Schneider (1989)
∅	Total porosity (−)	0.6	Bruce Harrison, personal communication (2017)
K_{sat}	Vertical matrix saturated hydraulic conductivity (mm/hr)	20	Hassler et al. (2011)
f_{max}	Maximum percolation rate (mm/hr)	20	Cheng et al. (2017)

(b) Land cover parameters	Descriptions	Forest	Pasture	References
I	Interception (%)	17	5	Zimmermann et al. (2013) and Niedzialek and Ogden (2012)
d	Top-layer thickness (cm)	20	12	Hassler et al. (2011) and Cheng et al. (2017)
$\frac{AT_{dry}}{AT_{wet}}$	Ratio of actual transpiration (AT), dry over wet seasons (−)	1.9	1.01	Mario Bretfeld, personal communication (2017)
D	Preferential flow layer thickness (m)	2.0	1.0	Jan Hendrickx and Bruce Harrison, personal communication (2017)
i_f	Infiltration capacity (mm/hr)	330	140	Ogden et al. (2014)
N_l	Lateral PFP number per grid cell	180	90	Shougrakpam et al. (2010) and Sarkar et al. (2012)
μ_l	Average lateral PFP diameter (mm)	3.0	1.5	Shougrakpam et al. (2010) and Sarkar et al. (2012)
N_v	Effective percolating vertical PFP number per grid cell	18	6	This study
μ_v	Average vertical PFP diameter (mm)	3.0	1.5	Cheng et al. (2017)

Note. PFP: preferential flow path.

were present (42% of forest and 58% of pasture). Note that these land cover percentages were slightly different from Ogden et al. (2013) due to a new land use interpretation.

The model input parameter values common to both land covers and their sources are listed in Table 2a. The specific parameter values for forest and pasture land covers are given in Table 2b. The model parameters that differed according to land covers are interception, ET, preferential flow layer thickness, top layer thickness, and lateral and vertical PFP characteristics.

Both the parameters for overall formulation and two land use types were quantitatively or semiquantitatively derived from field measurements or from literature. The actual annual ET depth for each study catchment was estimated based on a simple annual water budget calculation. According to Zimmermann et al. (2013) and Niedzialek & Ogden (2012), rainfall interception in forest and pasture land covers were 17% and 5%, respectively. The preferential flow layer thicknesses for forest and pasture were given as 2 and 1 m according to the root mass distribution in the study site (Jan Hendrickx & Bruce Harrison, personal communication, 2017) and time-lapse electrical resistivity tomography measurements during simulated rainfall experiments (Ogden et al., 2014). PFP parameters were derived from tropical data sources to the extent possible (Shougrakpam et al., 2010; Sarkar et al., 2012). The mean diameters of lateral and vertical macropores were assumed to be 3.0 mm for forest land cover (Sarkar et al., 2012; Shougrakpam et al., 2010). For pasture land cover, the mean diameters of lateral and vertical macropores were estimated as 1.5 mm (Sarkar et al., 2012; Shougrakpam et al., 2010). Given the importance of lateral macropores in partitioning between lateral drainage and vertical recharge to deep groundwater and in estimating the number of vertical PFPs, we performed a sensitivity analysis on the number and diameter of lateral macropores to evaluate effects of uncertainty in this parameter on the overall model performance. We varied the number of lateral PFPs in forest and pasture land covers from 10 to 200 and the diameter from 1 to 5 mm, (Sarkar et al., 2012; Shougrakpam et al., 2010).

A simple single linear reservoir model was used to simulate discharge of deep groundwater to streamflow by using equation (1).

$$q = K{\cdot}S \tag{1}$$

where q is the specific discharge to all the channel elements from the deep groundwater reservoir (L/T), K is the linear reservoir recession constant (T^{-1}), and S is the current groundwater reservoir storage (L). The linear reservoir recession constants were estimated by calibration from the observed runoff data (0.0012 h^{-1}, 0.0014 h^{-1}, and 0.0017 h^{-1} for the FOR, MOS, and PAS catchments, respectively).

2.3. Determination of Vertical PFP-Related Parameter From Field Data

The number of effective percolating vertical PFPs is the most difficult parameter to estimate. Cheng et al. (2017) concluded that these flow paths are almost entirely responsible for groundwater recharge. Cheng et al. (2017) calibrated a connectivity parameter to calculate this number. In this present study, however, instead of estimating another connectivity parameter, we used infiltration measurements at different scales to estimate the number of effective percolating vertical PFPs. Available multiscale infiltration measurements in different land covers included soil matrix infiltrability tests conducted using 9-cm diameter soil cores (Hassler et al., 2011) and infiltration measurements taken over 12-m^2 areas using rainfall simulator experiments (Ogden et al., 2014). Differences between these measurements, made at different scales, were used to estimate the vertical PFP number parameter for different land use types with the goal of minimizing the number of parameters calibrated. The rainfall rates during the rainfall simulator experiments involved three or four 750-L tanks of water applied on 12 m^2 of land surface over about 1 hr, yielding applied rainfall rates in the range of 200 to 400 mm/hr. Because these very high intensities of rainfall were applied during the rainfall simulator measurements and little overland flow was observed, we assumed that the soils were saturated and both lateral and vertical PFPs were activated under steady state conditions. Note that these assumptions allowed the use of the following simple water balance relationship for the irrigated plot (Figure 2b):

$$Q_{\text{input}} = Q_m + Q_v + Q_l \tag{2}$$

where Q_{input} is the input volume flow rate from the rainfall simulator (L^3/T), Q_m is the discharge through soil matrix (L^3/T), Q_v is the discharge through effective percolating vertical PFPs (L^3/T), and Q_l is the discharge through lateral macropores (L^3/T) in the top layer due to a perched groundwater table on the bottom of the top layer as shown in Figure 2b.

The input volume flow rate was calculated using the measured infiltration capacity from rainfall simulator experiments. The water flow in the soil matrix was computed using the Darcy's law. The volumetric flow rates in lateral and vertical macropores were calculated by applying Poiseuille's law in pipes (Sutera & Skalak, 1993). Equation (2) can then be rewritten as

$$i_f{\cdot}A = K_{\text{sat}}{\cdot}\left(A - \pi{\cdot}\sum_{k=1}^{N_v} {R_{vk}}^2\right){\cdot}\frac{\Delta h_v}{\Delta z} + \left(\frac{\rho g \pi}{8\mu}{\cdot}\sum_{k=1}^{N_v} {R_{vk}}^4\right){\cdot}\frac{\Delta h_v}{\Delta z} + \left(\frac{\rho g \pi}{8\mu}{\cdot}\sum_{k=1}^{N_l} {R_{lk}}^4\right){\cdot}\frac{\Delta h_l}{\Delta L} \tag{3}$$

where i_f is the infiltration capacity measured from rainfall simulator experiments (L/T), A is the catchment area (L^2), and $\frac{\Delta h_v}{\Delta z}$ is the hydraulic gradient in vertical direction, which is generated from the perched groundwater table that forms at the bottom of the top layer in the preferential flow layer and the gravity. The vertical hydraulic gradient is $\frac{\Delta h_v}{\Delta z} \geq 1$ because the depth of the perched groundwater table is small compared to the preferential flow layer thickness. The hydraulic gradient in the lateral direction $\frac{\Delta h_l}{\Delta L}$ is assumed to equal the land surface slope. In equation (3), K_{sat} is the soil matrix vertical saturated hydraulic conductivity (L/T), R_v is the vertical macropore radius (L), R_l is the lateral macropore radius (L), N_v is the number of effective percolating vertical PFPs that fully extend below the preferential flow layer and have the ability to move water downward quickly to recharge the deep groundwater reservoir, N_l is the number of lateral macropores in the top layer of the preferential flow layer, ρ is the water density (M/L^3), g is the gravitational acceleration (L/T^2), and μ is the water dynamic viscosity ($M \cdot L \cdot T$).

The soil matrix saturated hydraulic conductivity K_{sat} was set to be the median soil matrix infiltrability derived from the soil cores, that is, 2 cm/hr (Hassler et al., 2011). The diameter of lateral and vertical macropores and the number of lateral macropores were estimated from relevant literature for tropical settings (Sarkar et al., 2012; Shougrakpam et al., 2010) as discussed above and given in Table 2b. The infiltration capacity for forest land cover was estimated as 330 mm/hr (Table 2b) by averaging rainfall simulator experiment measurements

conducted on two different days. The infiltration capacity of pasture land cover was 140 mm/hr (Table 2b) by averaging measurements conducted on five different days. With these values inserted, the number of effective percolating vertical PFPs, N_v, was the only unknown parameter in equation (3). The calculated results of N_v, for both forest and pasture land covers, are listed in Table 2b.

2.4. Base Flow Separation

The digital filter developed by Eckhardt (2005) separated base flow from total runoff. Eckhardt's filter has two parameters, the filter parameter a and the maximum value of the base flow index BFI_{max}. The parameter a is determined from base flow recession analysis, while BFI_{max} is a nonmeasurable parameter estimated according to hydrogeological conditions. In this study, we adopted the approach proposed in Collischonn & Fan (2013) to estimate BFI_{max} using a backward filtering operation using observed streamflow data.

2.5. Water Budget Computations

The runoff efficiencies for various ranges of storm-total rainfall were calculated as the ratio of average direct runoff over average rainfall for the respective range during the simulated water year (Ogden et al., 2013). The depths for surface water storage, soil moisture storage, and deep groundwater storage for each study catchment were calculated by summing up the water volumes in the surface, preferential flow layer, and deep groundwater reservoir and dividing by the respective catchment area, respectively.

A dynamic perched groundwater table forms at the bottom of top layer in the preferential flow layer. The average transient groundwater table depth for each study catchment was calculated by summing up water volume perched at the bottom of the top layer in all grid cells and dividing by the respective catchment area. The flow capacity in the effective percolating vertical PFPs in the preferential flow layer was calculated by summing up the flow rates in all PFPs and dividing by the respective catchment area.

2.6. Model Assessment

Multiple objective criteria allowed evaluation of model performance against 15-min resolution hydrographs. These criteria included runoff Volume Error (VE), root-mean-square error (RMSE), and Nash-Sutcliffe efficiency calculated on two different variables: (1) the nontransformed modeled and observed discharge series (NSE), which emphasized the total runoff and the peak flows, and (2) the Nash-Sutcliffe efficiency calculated using the logarithm of the simulated and observed discharge series (NSE_{log}), which emphasized low flows (Samuel et al., 2012; Cheng et al., 2017). These four objective measures provided a range of indictors of model performance in terms of overall water balance, high flow, and low flow.

3. Results and Discussion

3.1. Model Performance Evaluation

Figure 3 shows measured and simulated hydrographs over the simulated period from 11 May 2011 to 19 May 2012 for the study catchments. The plots of observed and simulated cumulative runoff and scatterplots of both the observed and simulated runoffs together with the performance measures of VE, RMSE, and NSEs for the three study catchments are given in Figure 4. The distributions of runoff rate for both the observed and simulated daily hydrographs in the three study catchments are plotted in Figure 5.

Quantitatively, the absolute runoff Volume Errors (VEs) were below 3% for all three catchments: −0.04%, 2.25%, and −1.2% for the FOR, MOS, and PAS catchments, respectively (Figures 4a–4c). All the RMSEs were less than 0.05 mm/d (Figures 4a–4c). The overall streamflow patterns for all three study catchments were well simulated based on the NSE values of 0.7, 0.86, and 0.82 calculated from the nontransformed FOR, MOS, and PAS catchment hydrographs, respectively (Figures 4d–4f). The base flow characteristics of the three hydrographs were also simulated well, which was evident by the satisfactory performance NSE_{log} values of 0.7, 0.81, and 0.82 for the three catchments, respectively (Figures 4d–4f). The peak runoff rates agreed well with observations as can be seen from the 95th percentile in Figures 5a–5c for all three catchments.

Moreover, the simulation results that the PAS catchment produced higher peak runoff rates (Figure 5), more direct runoff (Table 3a), and higher storm runoff efficiencies (Table 3b) than the other two more forested catchments were consistent with the observations in small tropical catchments (e.g., Scott et al., 2005; Waterloo et al., 2007; Germer et al., 2010; Rodriguez et al., 2010). Using two sets of land use parameters informed by infiltration measures at different scales to estimate the number of effective percolating

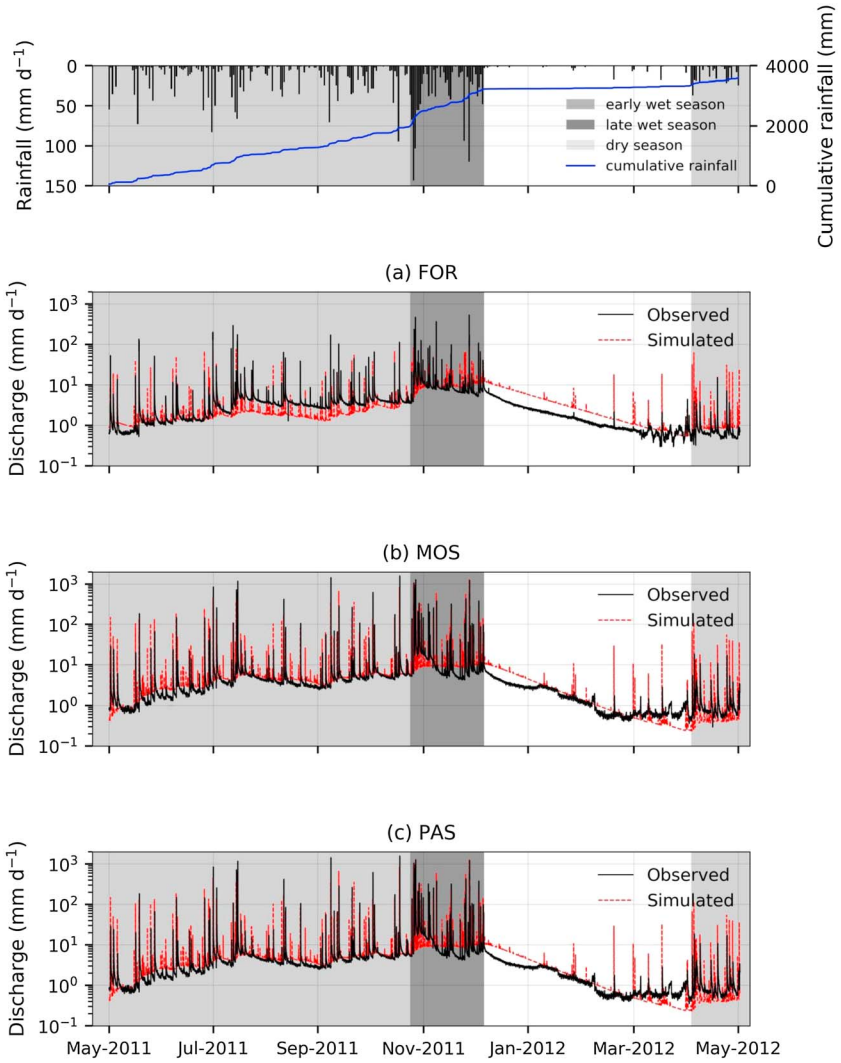

Figure 3. Comparison between the observed and simulated stream discharge for the period 11 May 2011 to 19 May 2012 for the three study catchments: (a) forest catchment (FOR), (b) mosaic catchment (MOS), and (c) pasture catchment (PAS).

vertical PFPs, the physically based model PFPMod demonstrated satisfactory skill at simulating both base flow and runoff peaks in the three catchments with distinct land covers.

The corresponding NSE values for the sensitivity analysis of the number and diameter of lateral PFPs ranged from 0.5 to 0.86, and NSE_{log} results varied from 0.52 to 0.82 for the three study catchments. The results demonstrated that as long as the parameters of lateral macropores were within the typical ranges presented in literature, satisfactory model performance could be achieved in terms of both total runoff and base flow.

3.2. Annual Base Flow

The recession parameter *a* of Eckhardt's filter was estimated as 0.96 using daily discharge data for all three study catchments, and the maximum values of the base flow index BFI_{max} were estimated as 0.83, 0.80, and 0.70 for the FOR, MOS, and PAS catchments, respectively. The model applications showed good agreements between simulations and observations in terms of annual base flow for each study catchment (Table 3a). Note that in our model conceptualization, the source of base flow was from the deep groundwater reservoir, which was recharged through vertical PFPs that allowed water to bypass the root zone soil matrix in the preferential flow layer and quickly move downward. While the total number of percolating vertical PFPs

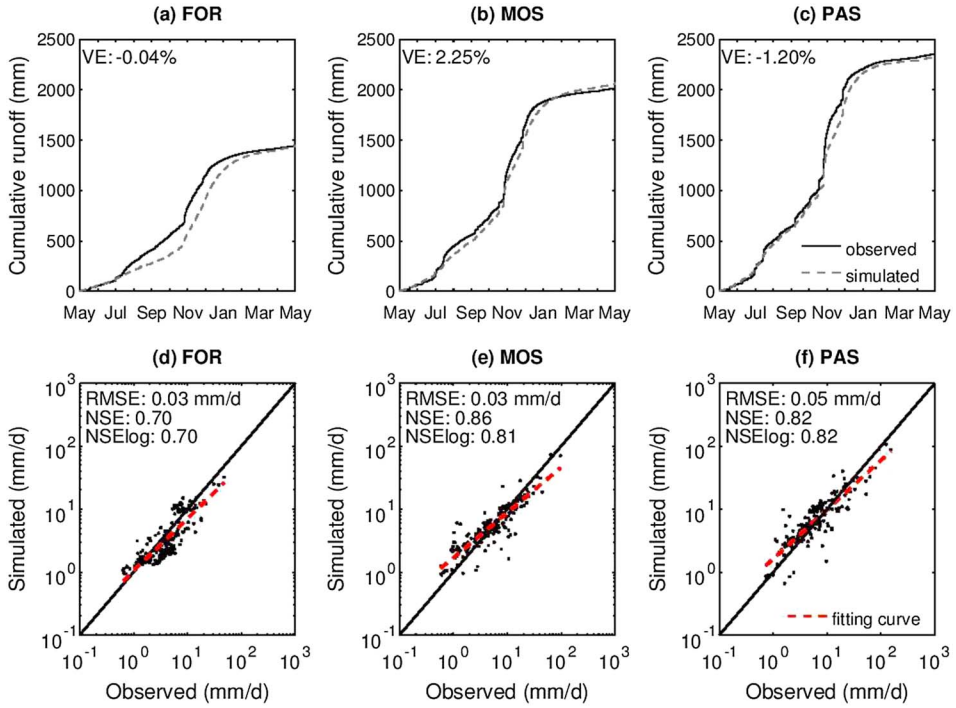

Figure 4. Cumulative runoff and scatterplots of the simulated and observed discharges and performance statistics (runoff Volume Error VE, root-mean-square error RMSE, Nash-Sutcliffe efficiency of nontransformed discharge values NSE, and the Nash-Sutcliffe efficiency for the logarithms of discharge data NSE_{log}) during the simulation period 11 May 2011 to 19 May 2012 for the three study catchments: (a and d) forest catchment (FOR), (b and e) mosaic catchment (MOS), and (c and f) pasture catchment (PAS). Notes: The equations used to calculate the performance statistics are as follows with the total number of data points m = 375: $VE = \left(\frac{R_{sim} - R_{obs}}{R_{obs}}\right) \times 100\%$, $RMSE = \sqrt{\frac{\Sigma_{i=1}^{m} \left(Q_{sim}^{i} - Q_{obs}^{i}\right)^2}{m.}}$ $NSE = 1 - \left(\frac{\Sigma_{i=1}^{m} \left(Q_{sim}^{i} - Q_{obs}^{i}\right)^2}{\Sigma_{i=1}^{m} \left(Q_{obs}^{i} - \overline{Q_{obs}}\right)^2}\right)$, $NSE_{log} = 1 - \left(\frac{\Sigma_{i=1}^{m} \left(\log Q_{sim}^{i} - \log Q_{obs}^{i}\right)^2}{\Sigma_{i=1}^{m} \left(\log Q_{obs}^{i} - \overline{\log Q_{obs}}\right)^2}\right)$ where R_{obs} and R_{sim} are observed and simulated annual runoffs, respectively; Q_{obs}^{i} and Q_{sim}^{i} are the observed and simulated discharges series, respectively; $\overline{Q_{obs}}$ is the average value of Q_{obs}^{i}; and m is the total number of data points.

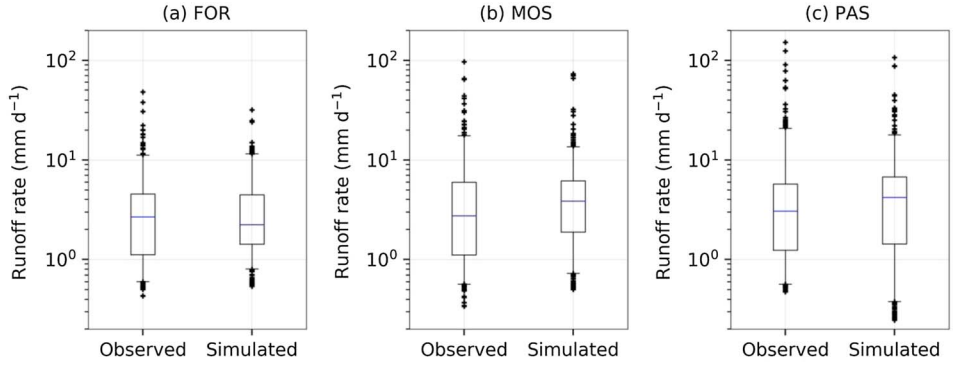

Figure 5. Runoff rates for observed and simulated discharge series for the three study catchments: (a) forest catchment (FOR), (b) mosaic catchment (MOS), and (c) pasture catchment (PAS) during the simulation period 11 May 2011 to 19 May 2012. The central bar is the median, the upper and lower limits of the box represent the 25th and 75th quantiles, while the whiskers represent the 5th and 95th percentiles. Symbols denote outliers below the 5th percentile or in excess of 95th percentile. The number of total data points is 375.

Table 3
(a) Annual Base Flow (R_b) and Annual Base Flow as a Percent of Annual Runoff (R_b/R_a) for the Three Study Catchments Over the Simulated Water Year From Both Observation and Simulation Results, (b) Runoff Efficiency for Various Rainfall Ranges Over the Simulated Water Year From Both Observation and Simulated Results, and (c) Annual Water Budget Components (Annual Runoff R_a, Actual Evapotranspiration AET, Interception I, Soil Moisture Storage Changes ΔS_{soil}, Deep Groundwater Storage Changes ΔS_{gw}, and Surface Water Storage Changes ΔS_{sur}) for the Three Study Catchments Over the Simulated Water Year From Model Simulation Results

(a) Annual base flow	FOR catchment		MOS catchment		PAS catchment	
	Observed (%)	Simulated (%)	Observed (%)	Simulated (%)	Observed (%)	Simulated (%)
R_b (mm)	1,155	1,159	1,518	1,477	1,413	1,402
R_b/R_a (%)	80%	80%	72%	72%	60%	60%
(b) Runoff efficiency	FOR catchment		MOS catchment		PAS catchment	
Storm rainfall range (mm)	Observed (%)	Simulated (%)	Observed (%)	Simulated (%)	Observed (%)	Simulated (%)
>1.00–3.16 (N = 4)	6.4	5.2	6.4	7.1	11.4	11.0
>3.16–10.0 (N = 58)	8.1	5.5	6.9	7.3	10.8	10.1
>10.0–31.6 (N = 53)	5.9	5.6	9.7	8.1	14.8	14.1
>31.6–100 (N = 33)	9.1	5.5	17.8	15.5	28.3	27.7
>100–316 (N = 4)	15.3	17.3	32.5	37.9	59.9	61.7
3.05–182 (N = 152)	8.9	7.1	14.7	16.1	25.0	26.1
(c) Simulated annual water budget components	FOR catchment		MOS catchment		PAS catchment	
R_a (mm)	1,442		2,056		2,319	
AET (mm)	1,507		1,118		950	
I (mm)	616		402		310	
ΔS_{soil} (mm)	27		20		17	
ΔS_{gw} (mm)	3.1		0.7		2.5	
ΔS_{sur} (mm)	0.8		2		−0.1	

Note. The FOR represents for forest, the MOS represents for mosaic, and the PAS represents for pasture. All the water budget component depth values are relative to the respective catchment area. The equation for runoff efficiency calculation is $E_r = \frac{\overline{\sum_{i=1}^{N} R_{di}}}{\sum_{i=1}^{N} P_i}$, where E_r is the runoff efficiency, N is the number of storm that fall into each rainfall range, and R_{di} and P_i are the direct runoff and rainfall of each storm, respectively.

ranged from less than 10 per model grid cell for the PAS catchment to only about 20 for the FOR catchment per model cell (Table 2b), their existence was essential to capture the observed base flow patterns.

The model results indicated that the contribution of base flow to annual runoff was 80%, 72%, and 60% in the FOR, MOS, and PAS catchments, respectively (Table 3a). These percentages were similar to the high base flow index results reported in Birkel et al. (2012) based on studies in Costa Rica and Beck et al. (2013) who studied 12 catchments in Puerto Rico.

3.3. Discussion of Annual and Seasonal Water Balances

The components of the simulated annual water balance are listed in Table 3c. Cumulative runoff, cumulative ET, surface water storage, soil moisture storage, and deep groundwater storage over the entire simulation period are shown in Figure 6. The results highlight the differences for the early wet season from May to early October, the late wet season from late October to December, and the dry season from January to April.

The FOR catchment generated the least annual runoff, especially during the late wet season (Figure 6a) because this catchment had the highest simulated interception and uptake of soil water for ET (Table 3c). The PAS catchment consistently produced the highest runoff during rainfall events compared to the other two catchments (Figure 6a).

In terms of simulated surface water storage, the variations in surface water in the PAS catchment were largest over the entire period (Figure 6c). The fractions of the catchments that produced overland flow during the early wet season were 0.1%, 3%, and 5% for the FOR, MOS, and PAS catchments, respectively. During the wet season, the simulated catchment area fractions with overland flow were 4%, 11%, and 21% in the three study catchments, respectively. The overland flow-generating fractions were less than 1% in all three study catchments during the dry season. The simulated results revealed that the PAS catchment with substantial

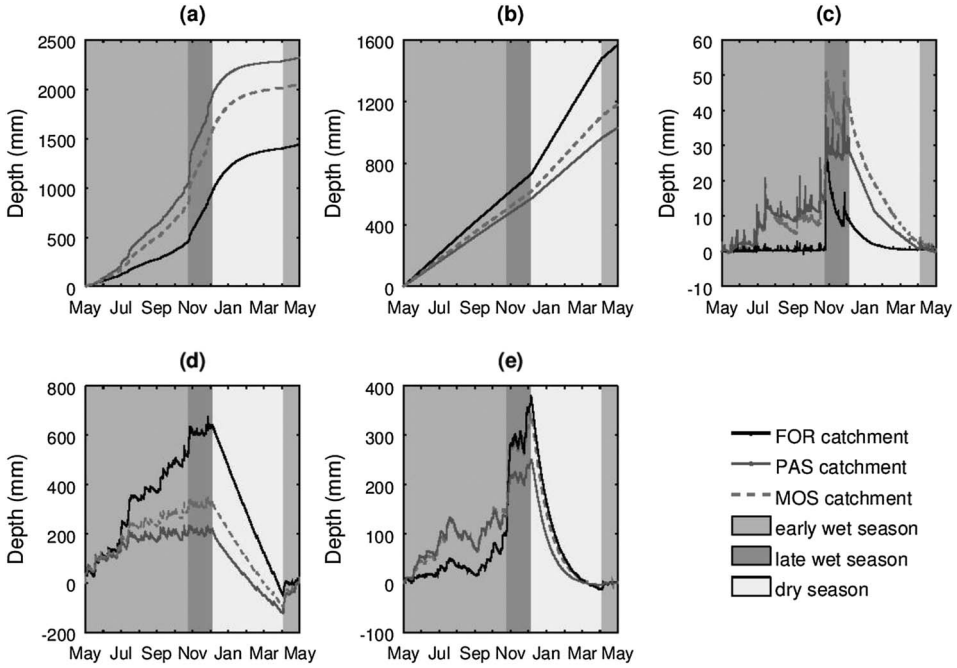

Figure 6. Water budget components (a) cumulative runoff, (b) cumulative evapotranspiration, (c) surface water storage, (d) soil moisture storage, and (e) deep groundwater storage during the simulation period 11 May 2011 to 19 May 2012 for the three study catchments from model simulation results.

pasture land cover had the highest possibility to produce overland flow, as also suggested by Hassler et al. (2011) and Ogden et al. (2013). These results further supported that overland flow was less likely to be a dominant contributor to runoff in the FOR catchment other than that through saturation-excess mechanism near streams during large rainfall events (Ogden et al., 2013).

The higher simulated water storage as soil moisture in the FOR catchment in the wet season (Figure 6d) is the main reason that it can satisfy more of the ET demand during the following dry season as seen in Figure 6b, which was consistent with the conclusion from von Randow et al. (2004) that the rate of moisture storage change in the forest was more rapid than that in the pasture at the start of the dry season. The FOR catchment had the largest deep groundwater storage at the end of the wet season (Figure 6e) and was thus able to consistently produce more base flow during the dry season compared to both the MOS and PAS catchments.

3.4. Discussion of Land Use Effects on Water Balance Dynamics

The average saturated thickness of a transient perched groundwater table above the bottom of the upper preferential flow layer together with the flow capacity of the effective percolating vertical PFPs in the preferential flow layer is shown in Figure 7. The simulation results provide insight into possible reasons for the observed catchment behaviors such as the forest sponge effect in the FOR catchment.

The simulated deep groundwater storage in the early wet season from May to early October suggested that the FOR catchment actually stored less water in the deep groundwater reservoir than the PAS and MOS catchments (Figure 6e). This was attributable to the fact that the FOR catchment had higher ET and more and larger lateral PFPs (Table 2b) as a result of abundant larger tree roots, which conducted throughflow downslope more quickly and resulted in a shallower average depth of simulated transient perched groundwater table than the other two catchments (Figure 7). Although the FOR catchment contained more vertical PFPs that can move more water downward to become deep groundwater recharge, these vertical PFPs did not reach their capacity in the early wet season with shallower simulated perched groundwater table depth (Figure 7a) due to the relatively lower rainfall intensity compared to late wet season. In addition, the shallower the perched water table, the fewer macropores were activated as demonstrated in Sarkar et al. (2012). Therefore, the flow capacity of lateral PFPs controlled the depth of the simulated transient perched groundwater table on the bottom of top layer, which in turn determined the amount of water available to deep

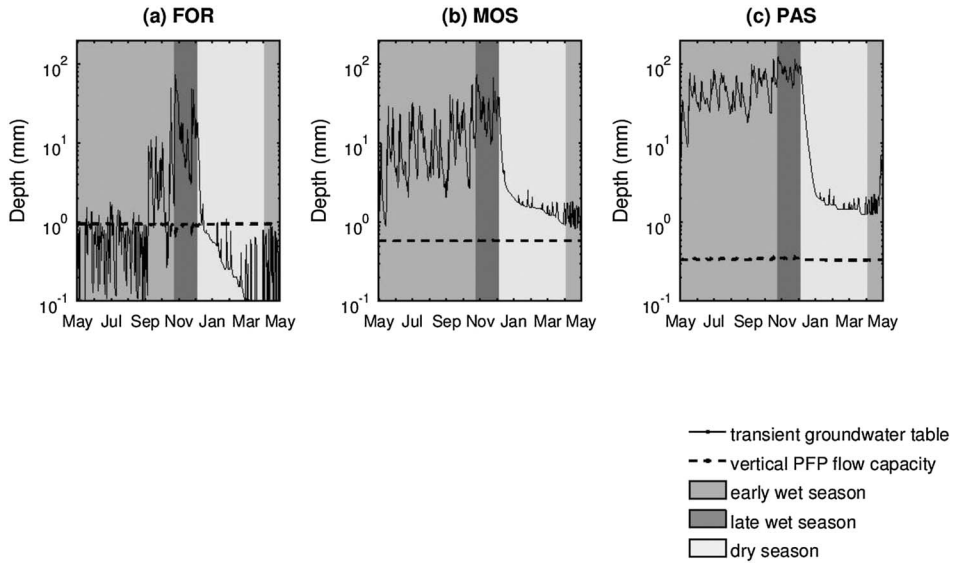

Figure 7. Depth of the transient groundwater table perched above the bottom of the top layer and flow capacity of the vertical preferential flow paths (PFPs) in the preferential flow layer during the simulation period 11 May 2011 to 19 May 2012 for the three study catchments from model simulation results: (a) forest catchment (FOR), (b) mosaic catchment (MOS), and (c) pasture catchment (PAS).

groundwater recharge during the early wet season. These transient, perched groundwater tables and their interplay with rapid preferential flow paths were also previously reported by Mulholland (1993), Scanlon et al. (2000), and Sarkar & Dutta (2014). These simulation results clearly illustrated that the lateral PFPs drain most water during the early wet season and highlighted the need to better quantify lateral macropore initiation and flow capacity.

However, during the late wet season from late October to December, due to the increased rainfall intensity, there were more occasions when the depth of the simulated transient perched groundwater table exceeded the vertical PFP flow capacity in all three catchments (Figure 7). In these occasions, all vertical PFPs may contribute to move water downward to deep groundwater recharge (Figure 7), leading to greater simulated groundwater recharge in the FOR catchment because of the greater total flow capacity of the vertical PFPs in forest land cover. During the late wet season, it was the vertical PFP flow capacity that dominated simulated deep groundwater recharge. Changing from the lateral PFP flow capacity-dominant mechanism to the vertical PFP flow capacity-dominant mechanism for simulated deep groundwater recharge highlighted the interplay between the vertical and lateral macropores under different land uses/land covers. The interplay played a significant role in regulating rainfall partition between quick flow through shallow lateral PFPs and deep groundwater recharge through vertical PFPs, which respectively manifested as peak flows during the wet season and sustained base flow during the dry season in tropical ecosystems.

Ogden et al. (2013) showed that the stored water was released to streams more slowly from the FOR catchment and resulted in higher dry-season base flow. However, it was difficult to quantitatively explain the reason behind this phenomenon due to the limited observed data without individual water balance components. The model structure and results in this study made it possible to analyze how individual water balance components interact in regulating water partition through different flow paths, especially in the subsurface. The model simulation results from the three study catchments with distinct land covers clearly demonstrated that the enhanced ability of forest land cover to recharge deep groundwater through more abundant vertical PFPs in the late wet season (Figure 6e and 7a) was responsible for the observed higher dry-season base flow in forested catchment. In addition to the fact that the simulated runoff rate (Figure 6) and surface water storage (Figure 6c) results corroborated the conclusion of higher runoff peak rates and runoff efficiencies in the PAS catchment reported by Ogden et al. (2013), the simulated results of soil moisture and deep groundwater storage further demonstrated that the greater ability of the forest land to store water as soil moisture and deep groundwater resulted in enhanced lateral drainage through more abundant plant

roots (Sarkar & Dutta, 2014) and produced less overland flow (Figure 6c) and direct runoff. In summary, through different biological effects that altered the characteristics of both lateral and vertical PFPs (Table 2b), forest and pasture land covers altered the hydrological behaviors differently, which could explain the observed forest sponge effect and the difference in storm runoff peaks and efficiencies.

4. Conclusions

This study applied a distributed and physically based model (Cheng et al., 2017) that we call PFPMod that explicitly accounts for lateral and vertical preferential flow paths (PFPs) to three adjacent catchments with distinctly different land use within the Panama Canal Watershed. The overarching objective was to better understand the mechanism by which land use/land cover affects the hydrological response of steep, lowland catchments in the seasonal tropics.

Model parameters were estimated using field measurements from the study catchments where possible. In the absence of observations, parameters were estimated from the literature. Multiple objective criteria were applied to evaluate the model performance in capturing peak and base flows in addition to satisfactorily simulating the annual water balance. Model runoff volume errors were less than 3% for all three catchments. Nash-Sutcliffe efficiency values for Q log (Q) were all greater than 0.7 for the three study catchments and in most cases were greater than 0.8. The satisfactory performance of the model compared with the observed data supported the two hypotheses that land use/land cover affects hydrological responses through its effects on the formation of PFPs and that core-scale measurements of matrix infiltrability and infiltration capacity measurements at the plot scale allow estimation of the number of vertical macropores that fully extend below the root zone.

Modeled changes in water balance components from early to late wet seasons at the three catchments with different land covers suggested that land use-dependent PFPs regulate runoff in tropical catchments. We found lateral downslope drainage through lateral PFPs due to the perched shallow groundwater table dominated during the early wet season. The higher rainfall in the late wet season and greater shallow groundwater depth in the upper soil layer satisfied the high flow capacity in vertical PFPs in forests, which recharged deep groundwater. These results together with the ET difference between forest and pasture land covers led us to conclude that the difference in peak runoff and the internal mechanism of the forest sponge effect, which means that forested tropical catchments can produce more base flow during the dry season than catchments with pastures, are attributable to land use/land cover-dependent PFPs.

The study increased predictive understanding of the role of land use/land cover in altering PFP characteristics and the effect of land use/land cover-dependent PFPs in regulating runoff generation in steep, lowland, and seasonal tropical catchments with saprolitic soils. The study also demonstrated the potential of a physically based distributed hydrological model with explicit consideration of PFPs related to different land use classes to simulate the hydrology of humid tropical catchments. The PFPMod provided insights and allowed us to examine the mechanism by which reforestation may help to restore ecosystem services and water security in similar tropical systems with distinct dry and wet seasons.

Acknowledgments
This work was funded by the U.S. National Science Foundation (NSF) EAR-1360384 WSC-Category 2 Collaborative Research: Planning and Land Management in a Tropical Ecosystem: Complexities of Land-use and Hydrology Coupling in the Panama Canal Watershed, and the Smithsonian Tropical Research Institute (STRI) Agua Salud Project. We acknowledge support by Jefferson Hall, Adriana Tapia, and Jorge Batista of STRI. Soil parameters and improved understanding were contributed by J. Bruce Harrison and Jan M. H. Hendrickx, through support from an NSF Innovations at the Nexus of Food, Energy and Water Systems (INFEWS) supplement. Rainfall simulator experiments were performed with the assistance of Alexis Mojica, Ed Kempema, Jason Regina, and Guy Litt. We thank Nels Frazier and Jason Regina for their assistance in programming. Graduate student support for integrated hydrological model testing was partially provided by the Wyoming Center for Environmental Hydrology and Geophysics (WyCEHG) funded by NSF EPS-1208909. Data and models used in this study are available at https://doi.org/10.15786/m20q35. The authors wish to express their great gratitude to Professor Sampurno Bruijnzeel and another anonymous reviewer for their constructive comments and suggestions, which significantly contributed to improving this paper.

References

Arcement, G. J., & Schneider, V. R. (1989). Guide for selecting Manning's roughness coefficients for natural channels and flood plains, United States Geological Survey Water-Supply Paper, 2339 (pp. 1–38). Denver, CO.

Bai, Z. G., Dent, D. L., Olsson, L., & Schaepman, M. E. (2008). Proxy global assessment of land degradation. *Soil Use and Management*, *24*(3), 223–234. https://doi.org/10.1111/j.1475-2743.2008.00169.x

Beck, H. E., Bruijnzeel, L. A., van Dijk, A. I. J. M., McVicar, T. R., Scatena, F. N., & Schellekens, J. (2013). The impact of forest regeneration on streamflow in 12 mesoscale humid tropical catchments. *Hydrology and Earth System Sciences*, *17*(7), 2613–2635. https://doi.org/10.5194/hess-17-2613-2013

Beck, H. E., van Dijk, A. I. J. M., Miralles, D. G., De Jeu, R. A. M., Bruijnzeel, L. A., McVicar, T. R., & Schellekens, J. (2013). Global patterns in base flow index and recession based on streamflow observations from 3394 catchments. *Water Resources Research*, *49*, 7843–7863. https://doi.org/10.1002/2013WR013918

Bernstein, L., Bosch P., Canziani O., Chen Z., Christ R., & Riahi K. (2008). IPCC, 2007: Climate change 2007—Synthesis report. IPCC.

Beven, K., & Germann, P. (2013). Macropores and water flow in soils revisited. *Water Resources Research*, *49*, 3071–3092. https://doi.org/10.1002/wrcr.20156

Birkel, C., Soulsby, C., & Tetzlaff, D. (2012). Modelling the impacts of land-cover change on streamflow dynamics of a tropical rainforest headwater catchment. *Hydrological Sciences Journal*, *57*(8), 1543–1561. https://doi.org/10.1080/02626667.2012.728707

Bonell, M., & Bruijnzeel, L. A. (Eds.) (2005). *Forests, water and people in the humid tropics: Past, present and future hydrological research for integrated land and water management*. Cambridge, UK: Cambridge University Press.

Bretfeld, M., Ewers, B. E., & Hall, J. S. (2018). Plant water use responses along secondary forest succession during the 2015–2016 El Niño drought in Panama. *New Phytologist*. https://doi.org/10.1111/nph.15071

Bruijnzeel, L. A. (1989). (De-)Forestation and dry season flow in the tropics: A closer look. *Journal of Tropical Forest Science*, 229–243.

Bruijnzeel, L. A. (2004). Hydrological functions of tropical forests: Not seeing the soil for the trees? *Agriculture, Ecosystems and Environment*, *104*(1), 185–228. https://doi.org/10.1016/j.agee.2004.01.015

Burgess, S. S., Adams, M. A., Turner, N. C., Beverly, C. R., Ong, C. K., Khan, A. A., & Bleby, T. M. (2001). An improved heat pulse method to measure low and reverse rates of sap flow in woody plants. *Tree Physiology*, *21*, 589–598.

Chappell, N. A. (2010). Soil pipe distribution and hydrological functioning within the humid tropics: A synthesis. *Hydrological Processes*, *24*(12), 1567–1581. https://doi.org/10.1002/hyp.7579

Chappell, N. A., Franks, S. W., & Larenus, J. (1998). Multi-scale permeability estimation for a tropical catchment. *Hydrological Processes*, *12*(9), 1,507–1,523. https://doi.org/10.1002/(SICI)1099-1085(199807)12:9<1507::AID-HYP653>3.0.CO;2-J

Chappell, N. A., Tych, W., Chotai, A., Bidin, K., Sinun, W., & Chiew, T. H. (2007). BARUMODEL: Combined Data Based Mechanistic models of runoff response in a managed rainforest catchment. *Forest Ecology and Management*, *224*(1–2), 58–80. https://doi.org/10.1016/j.foreco.2005.12.008

Cheng, Y., Ogden, F. L., & Zhu, J. (2017). Earthworms and tree roots: A model study of the effect of preferential flow paths on runoff generation and groundwater recharge in steep, saprolitic, tropical lowland catchments. *Water Resources Research*, *53*, 5400–5419. https://doi.org/10.1002/2016WR020258

Collischonn, W., & Fan, F. M. (2013). Defining parameters for Eckhardt's digital baseflow filter. *Hydrological Processes*, *27*(18), 2614–2622. https://doi.org/10.1002/hyp.9391

Colloff, M. J., Pullen, K. R., & Cunningham, S. A. (2010). Restoration of an ecosystem function to revegetation communities: The role of invertebrate macropores in enhancing soil water infiltration. *Restoration Ecology*, *18*(SUPPL. 1), 65–72. https://doi.org/10.1111/j.1526-100X.2008.00439.x

Davis, S. H., Vertessy, R. A., & Silberstein, R. P. (1999). The sensitivity of a catchment model to soil hydraulic properties obtained by using different measurement techniques. *Hydrological Processes*, *13*(5), 677–688.

Eckhardt, K. (2005). How to construct recursive digital filters for baseflow separation. *Hydrological Processes*, *19*(2), 507–515. https://doi.org/10.1002/hyp.5675

Gardner, C. B., Litt, G. F., Lyons, W. B., & Ogden, F. L. (2017). Evidence for the activation of shallow preferential flow paths in a tropical Panama watershed using germanium and silicon. *Water Resources Research*, *53*, 8533–8553. https://doi.org/10.1002/2017WR020429

Germer, S., Neill, C., Krusche, A. V., & Elsenbeer, H. (2010). Influence of land-use change on near-surface hydrological processes: Undisturbed forest to pasture. *Journal of Hydrology*, *380*(3–4), 473–480. https://doi.org/10.1016/j.jhydrol.2009.11.022

Ghimire, C. P., Bruijnzeel, L. A., Lubczynski, M. W., & Bonell, M. (2014). Negative trade-off between changes in vegetation water use and infiltration recovery after reforesting degraded pasture land in the Nepalese Lesser Himalaya. *Hydrology and Earth System Sciences*, *18*(12), 4933–4949. https://doi.org/10.5194/hess-18-4933-2014

Graham, E. A., Mulkey, S. S., Kitajima, K., Phillips, N. G., & Wright, S. J. (2003). Cloud cover limits net CO_2 uptake and growth of a rainforest tree during tropical rainy seasons. *Proceedings of the National Academy of Sciences*, *100*, 572–576.

Guo, L., & Lin, H. (2017). Addressing two bottlenecks to advance the understanding of preferential flow in soils. *Advances in Agronomy* (1st ed., pp. 147). Cambridge, MA: Elsevier Inc. https://doi.org/10.1016/bs.agron.2017.10.002

Hassler, S. K., Zimmermann, B., van Breugel, M., Hall, J. S., & Elsenbeer, H. (2011). Recovery of saturated hydraulic conductivity under secondary succession on former pasture in the humid tropics. *Forest Ecology and Management*, *261*(10), 1634–1642. https://doi.org/10.1016/j.foreco.2010.06.031

Krishnaswamy, J., Bonell, M., Venkatesh, B., Purandara, B. K., Lele, S., Kiran, M. C., et al. (2012). The rain-runoff response of tropical humid forest ecosystems to use and reforestation in the Wwestern Ghats of India. *Journal of Hydrology*, *472–473*, 216–237. https://doi.org/10.1016/j.jhydrol.2012.09.016

Krishnaswamy, J., Bonell, M., Venkatesh, B., Purandara, B. K., Rakesh, K. N., Lele, S., et al. (2013). The groundwater recharge response and hydrologic services of tropical humid forest ecosystems to use and reforestation: Support for the "infiltration-evapotranspiration trade-off hypothesis". *Journal of Hydrology*, *498*, 191–209. https://doi.org/10.1016/j.jhydrol.2013.06.034

Lacombe, G., Ribolzi, O., De Rouw, A., Pierret, A., Latsachak, K., Silvera, N., et al. (2016). Contradictory hydrological impacts of afforestation in the humid tropics evidenced by long-term field monitoring and simulation modelling. *Hydrology and Earth System Sciences*, *20*(7), 2691–2704. https://doi.org/10.5194/hess-20-2691-2016

Lai, W., Ogden, F. L., Steinke, R. C., & Talbot, C. A. (2015). An efficient and guaranteed stable numerical method for continuous modeling of infiltration and redistribution with a shallow dynamic water table. *Water Resources Research*, *51*, 1514–1528. https://doi.org/10.1002/2014WR016487

Li, K. Y., Coe, M. T., Ramankutty, N., & Jong, R. D. (2007). Modeling the hydrological impact of land-use change in West Africa. *Journal of Hydrology*, *337*(3–4), 258–268. https://doi.org/10.1016/j.jhydrol.2007.01.038

Litt, G. F., Gardner, C. B., Ogden, F. L., & Lyons, W. B. (2015). Hydrologic tracers and thresholds: A comparison of geochemical techniques for event-based stream hydrograph separation and flowpath interpretation across multiple land covers in the Panama Canal Watershed. *Applied Geochemistry*, *63*, 507–518. https://doi.org/10.1016/j.apgeochem.2015.04.003

Mallants, D., Mohanty, B. P., Vervoort, A., & Feyen, J. (1997). Spatial analysis of saturated hydraulic conductivity in a soil with macropores. *Soil Technology*, *10*(2), 115–131. https://doi.org/10.1016/S0933-3630(96)00093-1

Marshall, D. C. (1958). Measurement of sap flow in conifers by heat transport. *Plant Physiology*, *33*(6), 385–396. https://doi.org/10.1104/pp.33.6.385

Meinzer, F. C., Goldstein, G., & Andrade, J. L. (2001). Regulation of water flux through tropical forest canopy trees: Do universal rules apply? *Tree Physiology*, *21*(January), 19–26.

Meng, C., Niu, J., Li, X., Luo, Z., Du, X., Du, J., et al. (2016). Quantifying soil macropore networks in different forest communities using industrial computed tomography in a mountainous area of North China. *Journal of Soils and Sediments*, (June), 1–14. https://doi.org/10.1007/s11368-016-1441-2

Mulholland, P. J. (1993). Hydrometric and stream chemistry evidence of three storm flowpaths in Walker Branch Watershed. *Journal of Hydrology*, *151*(2–4), 291–316. https://doi.org/10.1016/0022-1694(93)90240-A

Niedzialek, J. M., & Ogden, F. L. (2012). First-order catchment mass balance during the wet season in the Panama Canal Watershed. *Journal of Hydrology*, *462–463*, 77–86. https://doi.org/10.1016/j.jhydrol.2010.07.044

Noguchi, S., Nik, A. R., Kasran, B., Tani, M., & Sammori, T. (1997). Soil physical properties and preferential flow pathwats in tropical rain forest, Bukit Tarek, Pennisular Malaysia. *Journal of Forest Research*, *2*, 115–120.

Noguchi, S., Tsuboyama, Y., Sidle, R. C., & Hosoda, I. (1999). Morphological characteristics of macropores and the distribution of preferential flow pathways in a forested slope segment. *Soil Science Society of America Journal*, *63*(5), 1413–1423.

Ogden, F. L., Allen, M. B., Lai, W., Zhu, J., Seo, M., Douglas, C. C., & Talbot, C. A. (2017). The soil moisture velocity equation. *Journal of Advances in Modeling Earth Systems*, *9*, 1473–1487. https://doi.org/10.1002/2017MS000931

Ogden, F. L., Creel, J. N., Kempema, E. W., & Crouch, T. D. (2017). Sedimentation effects on triangular short-crested flow-measurement weirs. *Journal of Hydrologic Engineering*, *22*(8), 04017020. https://doi.org/10.1061/(ASCE)HE.1943-5584.0001528

Ogden, F. L., Crouch, T. D., Stallard, R. F., & Hall, J. S. (2013). Effect of land cover and use on dry season river runoff, runoff efficiency, and peak storm runoff in the seasonal tropics of Central Panama. *Water Resources Research*, *49*, 8443–8462. https://doi.org/10.1002/2013WR013956

Ogden, F. L., Lai, W., Steinke, R. C., Zhu, J., Talbot, C. A., & Wilson, J. L. (2015). A new general 1-D vadose zone flow solution method. *Water Resources Research*, *51*, 4282–4300. https://doi.org/10.1002/2015WR017126

Ogden, F. L., Mojica A., Kempema E. W., Briceno J. C., & Regina J. (2014). Diagnosing hydrologic flow paths in forest and pasture land uses within the Panama Canal Watershed using simulated rainfall and electrical resistivity tomography. Paper presented at American Geophysical Union Fall Meeting, 15–19 December, H21F-0795, San Francisco, CA.

Peel, M., Kruger, J. M., & MacFadyen, S. (2007). Woody vegetation of a mosaic of protected areas adjacent to the Kruger National Park, South Africa. *Journal of Vegetation*, *18*(6), 807–814. Retrieved from https://onlinelibrary.wiley.com/doi.org/10.1111/j.1654-1103.2007.tb02597.x/full

Ray, D. K., Nair, U. S., Lawton, R. O., Welch, R. M., & Pielke, R. A. (2006). Impact of land use on Costa Rican tropical montane cloud forests: Sensitivity of orographic cloud formation to deforestation in the plains. *Journal of Geophysical Research*, *111*, D02108. https://doi.org/10.1029/2005JD006096

Rodriguez, D. A., Tomasella, J., & Linhares, C. (2010). Is the forest conversion to pasture affecting the hydrological response of Amazonian catchments? Signals in the Ji-Parana Basin. *Hydrological Processes*, *24*(10), 1254–1269. https://doi.org/10.1002/hyp.7586

Samuel, J., Coulibaly, P., & Metcalfe, R. A. (2012). Identification of rainfall–runoff model for improved baseflow estimation in ungauged basins. *Hydrological Processes*, *26*(3), 356–366. https://doi.org/10.1002/hyp.8133

Sarkar, R., Asce, S. M., & Dutta, S. (2012). Field investigation and modeling of rapid subsurface stormflow through preferential pathways in a vegetated hillslope of Northeast India. *Journal of Hydrologic Engineering*, *17*(February), 333–341. https://doi.org/10.1061/(ASCE)HE.1943-5584.0000431

Sarkar, R., & Dutta, S. (2014). Parametric study of a physically-based, plot-scale hillslope hydrological model through virtual experiments. *Hydrological Sciences Journal*, *60*(3), 448–467. https://doi.org/10.1080/02626667.2014.897407

Sarkar, R., Dutta, S., & Dubey, A. K. (2015). An insight into the runoff generation processes in wet sub-tropics: Field evidences from a vegetated hillslope plot. *Catena*, *128*, 31–43. https://doi.org/10.1016/j.catena.2015.01.006

Sarkar, R., Dutta, S., & Panigrahy, S. (2008). Effect of scale on infiltration in a macropore-dominated hillslope. *Current Science*, *94*(4), 490–494.

Scanlon, T. M., Raffensperger, J. P., Hornberger, G. M., & Clapp, R. B. (2000). Shallow subsurface storm flow in a forested headwater catchment: Observations and modeling using a modified TOPMODEL. *Water Resources Research*, *36*, 2,575–2,586. https://doi.org/10.1029/2000WR900125

Schellekens, J. (2000). Hydrological processes in a humid tropical rain forest: A combined experimental and modelling approach, (PhD thesis), Department of Earth Science, Vrije University, Amsterdam.

Schwendenmann, L., Pendall, E., Sanchez-Bragado, R., Kunert, N., & Hölscher, D. (2015). Tree water uptake in a tropical plantation varying in tree diversity: Interspecific differences, seasonal shifts and complementarity. *Ecohydrology*, *8*(1), 1–12. https://doi.org/10.1002/eco.1479

Scott, D. F., Bruijnzeel, L. A., & Mackensen, J. (2005). The hydrological and soil impacts of forestation in the tropics. In M. Bonell & L. A. Bruijnzeel (Eds.), *Forests, water and people in the humid tropics* (pp. 622–651). Cambridge, UK: Cambridge University Press.

Shougrakpam, S., Sarkar, R., & Dutta, S. (2010). An experimental investigation to characterise soil macroporosity under different land use and land covers of northeast India. *Journal of Earth System Science*, *119*(5), 655–674. https://doi.org/10.1007/s12040-010-0042-5

Tobón, C., Bruijnzeel, L. A., Frumau, K. F. A., & Calvo-Alvarado, J. C. (2010). Changes in soil physical properties after conversion of tropical montane cloud forest to pasture in northern. *Tropical Montane Cloud Forests: Science for Conservation and Management*, 502–515. https://doi.org/10.1017/CBO9780511778384.054

Vertessy, R. A., & Elsenbeer, H. (1999). Distributed modeling of storm flow generation in an Amazonian rain forest catchment: Effects of model parameterization. *Water Resources Research*, *35*, 2173–2187.

Von Randow, C., Manzi, A. O., Kruijt, B., de Oliveira, P. J., Zanchi, F. B., Silva, R. L., et al. (2004). Comparative measurements and seasonal variations in energy and carbon exchange over forest and pasture in South West Amazonia. *Theoretical and Applied Climatology*, *78*(1–3), 5–26. https://doi.org/10.1007/s00704-004-0041-z

Waterloo, M. J., Schellekens, J., Bruijnzeel, L. A., & Rawaqa, T. T. (2007). Changes in catchment runoff after harvesting and burning of a Pinus caribaea plantation in Viti Levu, Fiji. *Forest Ecology and Management*, *251*(1), 31–44. https://doi.org/10.1016/j.foreco.2007.06.050

Wolf, S., Eugster, W., Majorek, S., & Buchmann, N. (2011). Afforestation of tropical pasture only marginally affects ecosystem-scale evapotranspiration. *Ecosystems*, *14*(8), 1264–1275. https://doi.org/10.1007/s10021-011-9478-y

Wu, W., Hall, C. A., & Scatena, F. N. (2007). Modelling the impact of recent land-cover changes on the stream flows in northeastern Puerto Rico. *Hydrological Processes*, *21*(21), 2944–2956. https://doi.org/10.1002/hyp.6515

Zimmermann, B., Elsenbeer, H., & De Moraes, J. M. (2006). The influence of land-use changes on soil hydraulic properties: Implications for runoff generation. *Forest Ecology and Management*, *222*(1–3), 29–38. https://doi.org/10.1016/j.foreco.2005.10.070

Zimmermann, B., Zimmermann, A., Scheckenbach, H. L., Schmid, T., Hall, J. S., & van Breugel, M. (2013). Changes in rainfall interception along a secondary forest succession gradient in lowland Panama. *Hydrology and Earth System Sciences*, *17*(11), 4659–4670. https://doi.org/10.5194/hess-17-4659-2013

Zou, X., & Gonzalez, G. (1997). Changes in earthworm density and community structure during secondary succession in abandoned tropical pastures. *Soil Biology and Biochemistry*, *29*(3–4), 627–629. https://doi.org/10.1016/S0038-0717(96)00188-5

Zwartendijk, B. W., van Meerveld, H. J., Ghimire, C. P., Bruijnzeel, L. A., Ravelona, M., & Jones, J. P. G. (2017). Rebuilding soil hydrological functioning after swidden agriculture in eastern Madagascar. *Agriculture, Ecosystems & Environment*, *239*, 101–111. https://doi.org/10.1016/j.agee.2017.01.002